Sensitivity of Pacific Ocean Tropical Instability Waves to Initial Conditions

JÉRÔME VIALARD

European Centre for Medium-Range Weather Forecasts, Reading, United Kingdom, and Laboratoire d'Océanographie Dynamique et de Climatologie, Paris, France

CHRISTOPHE MENKES

Laboratoire d'Océanographie Dynamique et de Climatologie, Paris, France

DAVID L. T. ANDERSON AND MAGDALENA ALONSO BALMASEDA

European Centre for Medium-Range Weather Forecasts, Reading, United Kingdom

(Manuscript received 15 February 2002, in final form 12 July 2002)

ABSTRACT

Tropical instability waves (TIWs) appear as monthly oscillations of the currents, sea level, and sea surface temperature of the eastern equatorial Pacific. They are understood as unstable waves feeding on the kinetic and potential energy of the mean currents. A general circulation model is shown to reproduce the main features associated with TIWs. It is then used to investigate the dynamical regime of TIWs, by assessing their sensitivity to oceanic initial conditions. Locally in space and time, small perturbations can grow enough to modify significantly the phase of the TIW field, suggesting some chaotic behavior. When considered over the whole active TIW region, however, the phases of the perturbed and unperturbed experiments remain in agreement. This suggests that TIW activity in this model is more consistent with a limit cycle behavior than with fully developed turbulence and that irregular behavior of TIWs mostly stems from external forcing by the wind. A stronger result is that TIWs in experiments starting from very different initial conditions come back into phase after a few years. This is consistent with the suggestion that TIWs might be phase-locked to the wind forcing. Quiescent periods of the TIW's cycle play an important role in the decay of TIW's phase disagreement but cannot explain the phase-locking mechanism entirely. The implications of these results and their sensitivity to the forcing are discussed.

1. Introduction

Tropical instability waves (hereinafter TIWs) are common to the Pacific and Atlantic oceans. They appear on spaceborne sea surface temperature (SST) measurements (Legeckis 1977) as large-scale westward-propagating oscillations of the temperature front separating cold water of the equatorial upwelling from warmer water to the north. They are associated with monthly period variability in sea level (Perigaud 1990; Weidman et al. 1999), as well as in zonal and meridional currents north of the equator. Recent observations show that these features are associated with anticyclonic vortices centered at about 4°N (Flament et al. 1996; Kennan and Flament 2000; Menkes et al. 2002). At the equator, there is a marked variability in the meridional currents at a 20-day period (Halpern et al. 1988; Halpern 1989). TIWs are important in the heat and momentum budget of the cold tongue (Swenson and Hansen 1999; Vialard et al. 2001) and are associated with strong biological activity (Menkes et al. 2002; Chavez et al. 1999; Murray et al. 1994).

There is no consensus on the instability mechanisms that give rise to TIWs (Weidman et al. 1999). Some studies suggest that barotropic instability of the shear region between the North Equatorial Countercurrent and South Equatorial Current could be important (Cox 1980), while others stress the importance of the shear between the Equatorial Undercurrent and the South Equatorial current (Luther and Johnson 1990; Qiao and Weisberg 1998; McCreary and Yu 1992). Other processes (such as baroclinic, Kelvin–Helmholtz or frontal instability) may also contribute to TIWs (Luther and Johnson 1990; McCreary and Yu 1992; Masina et al. 1999). Several studies suggest that the monthly variations north of the equator might arise from a different dynamical process than the meridional current oscilla-

Corresponding author address: J. Vialard, Laboratoire d'Océanographie Dynamique et de Climatologie, UMR CNRS, IRD, Université Pierre et Marie Curie, 4 Place Jussieu, 75252 Paris, Cedex 05, France.
E-mail: jv@lodyc.jussieu.fr

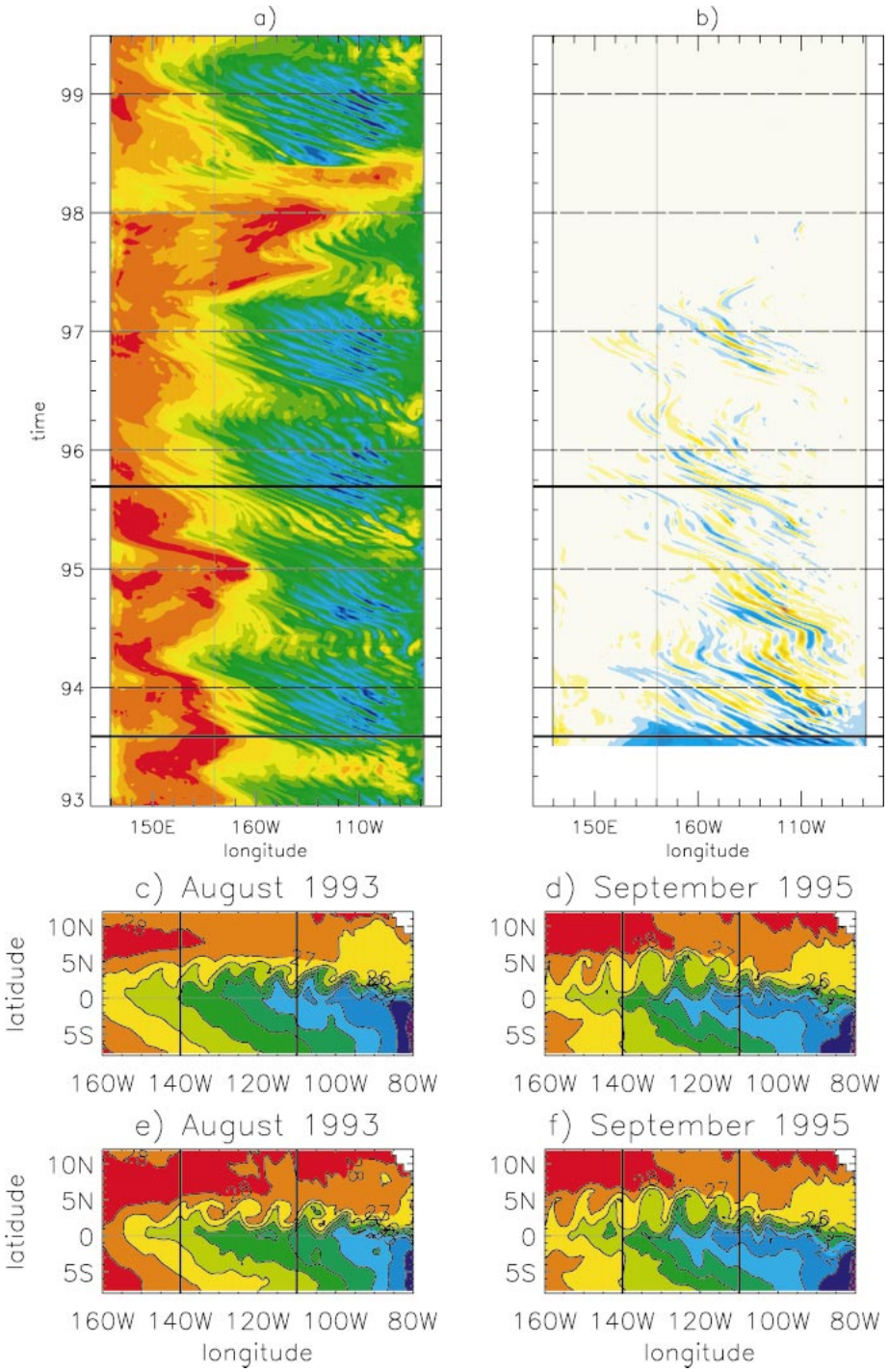

FIG. 1. Time–longitude section along 2°N: (a) SST of expt REF and (b) difference between the SST of expt REF and a sensitivity experiment restarting in Jul 1993 from the REF 1993–96 average; (c), (e) snapshots of the SST in Aug 1993 and (d), (f) Sep 1995. Here, (c) and (d) show expt REF, whereas the (e), (f) show the perturbation experiment. Note that the TIWs are largely decorrelated between the REF and perturbation experiments in Aug 1993 but have come back into phase by Sep 1995.

TABLE 1. Main experiments used in this study. Some other experiments (in particular initial conditions perturbation experiments) are described in the text.

Expt	Description
REF	Reference experiment: 1993–99, observed wind stress
SCY	Seasonal cycle experiment: 1993–96 average seasonal cycle wind stress
CST	Constant winds experiment: 1993–96 average wind stress

tions near the equator (Donohue and Wimbush 1998; Kennan and Flament 2000; Masina et al. 1999).

Despite this absence of consensus about the energy source, it is clear that TIWs are the result of an instability. Each year around June, the background oceanic flow becomes unstable. If TIWs were developing through amplification of small random perturbations of the background flow, one would expect their phase to be random. In particular, it should be highly sensitive to oceanic initial conditions and different in two model experiments starting from slightly different initial conditions. Two experiments run with the Laboratoire d'Océanographie Dynamique et de Climatologie (LODYC) Ocean General Circulation Model (Madec et al. 1999) show that this is not necessarily the case (Fig. 1). The model is run first using realistic forcing for the 1993–99 period (Vialard et al. 2001) and rerun starting from different initial conditions (restarted in July 1993 from the 1993–96 average of the previous run). As expected, TIWs are initially completely uncorrelated in the reference and perturbation experiments. After a few years, however, the TIW phases in the two experiments converge (Figs. 1b and 1e,f). To explain this, Allen et al. (1995) suggested that the development of TIWs is phase locked to the background flow fluctuations induced by intraseasonal wind variability. Benestad et al. (2001) showed that TIWs phase in their model was shifted by one week when they shifted the intraseasonal variability of the wind forcing by the same amount. However, none of these studies proposed an exact mechanism for this phase locking nor investigated in detail the sensitivity of modeled TIWs to initial conditions.

The sensitivity to initial conditions is intimately linked to the regime of the dynamical system (see, e.g., Strogatz 1994 for a textbook on dynamical systems and chaos). Self-sustained oscillations like TIWs can be the result of a stable limit cycle or of chaotic regime. In the first case, the oscillations are regular (but can become irregular under the effect of external forcing) and do not display strong sensitivity to initial conditions (i.e., a small perturbation of the limit cycle trajectory will not result in a radically different phase of the oscillations in the perturbed trajectory). In the chaotic regime, the system will display highly irregular (nonperiodic) oscillations on its own and strong sensitivity to

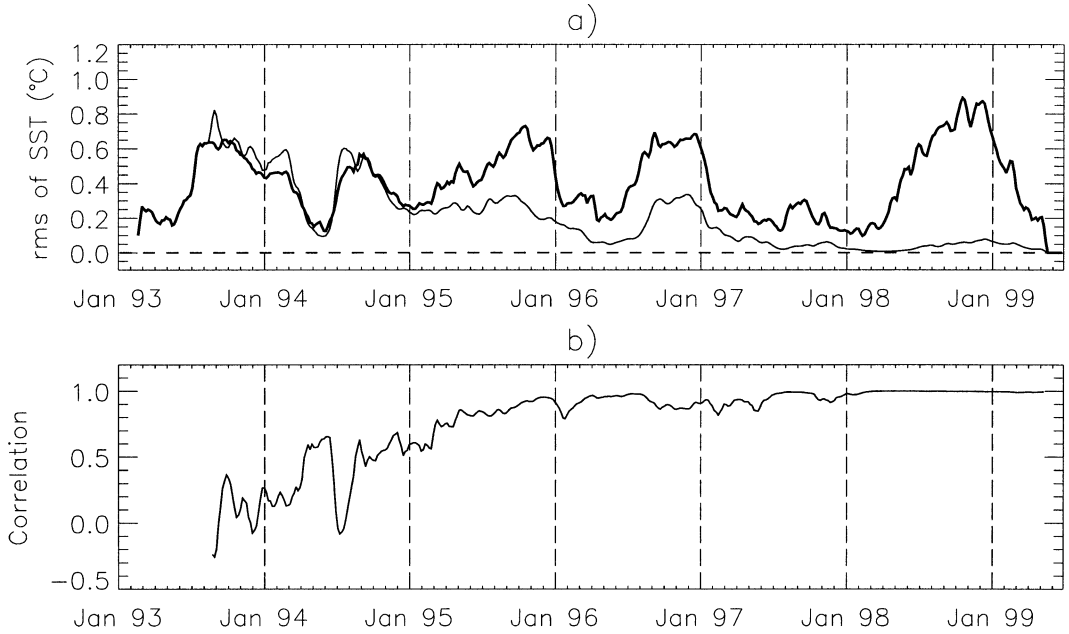

FIG. 2. (a) The thick line shows the level of activity of tropical instability waves in expt REF (shown in Fig. 1a). It is estimated by taking the spatial rms of the 50-day high-pass filtered SST over the 0°–4°N, 100°–160°W region. The thin line in (a) shows the phase and amplitude agreement of TIWs in expt REF and an experiment restarting in Jul 1993 from the REF 1993–96 average (cf Fig. 1). It is estimated by taking the rms of the 50-day high-pass filtered SST difference between the two experiments over the region defined above. When the thin curve has a small value relative to the thick curve, it indicates that the TIW phase and amplitude are similar in the REF and perturbed experiments. (b) The spatial correlation of the 50-day high-pass filtered SST of the two experiments in the same region.

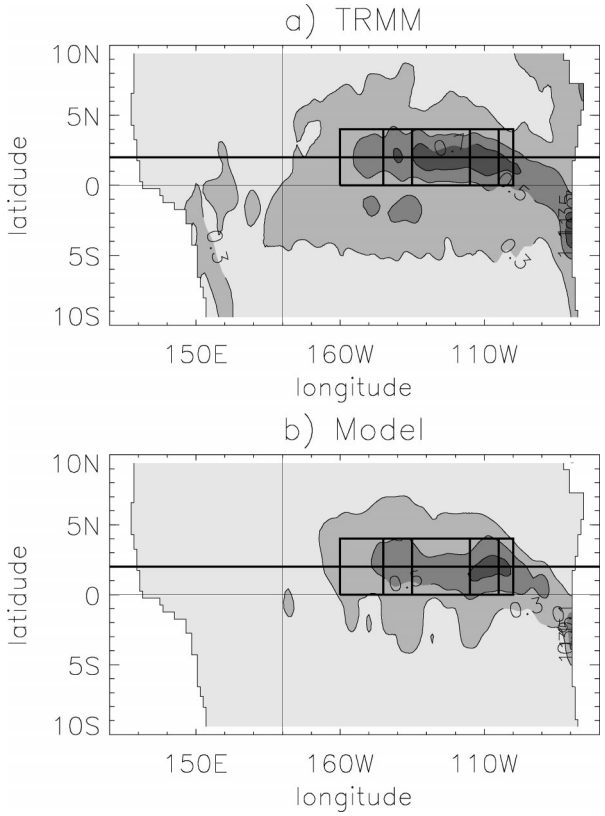

FIG. 3. Maps of the rms of 50-day high-pass filtered weekly SST for (a) TRMM SST and (b) model SST. The contour interval is 0.2°C. The horizontal thick line at 2°N indicates the latitude of the time section of Fig. 4. The 0°–4°N, 100°–160°W region is outlined for future reference.

initial conditions (i.e., a small perturbation to a trajectory on the attractor will result in exponential growth of the differences between the perturbed and unperturbed trajectories). In this paper, we will explore the dynamical regime of TIWs in realistic simulations of the tropical Pacific by investigating the sensitivity of TIWs to initial conditions.

We will first demonstrate that the LODYC model simulates most of the observed properties of TIWs (section 3). We will then investigate the sensitivity of TIWs to ocean initial conditions by performing perturbation experiments (section 4). It is shown that small perturbations to the model initial conditions can locally disrupt the phase and amplitude of the TIWs but that the agreement between the perturbed and unperturbed experiments over the TIW region as a whole remains good. In section 5, the sensitivity of TIWs to large perturbations of the oceanic initial conditions is examined. It is found that large perturbations initially disrupt the TIW field but that phase and amplitude agreement are recovered after 2–3 years. The role of quiescent phases of the TIWs activity seasonal cycle in this behavior is discussed, and it is concluded that TIWs must be phase locked to the wind forcing to explain this. In section 6, the main results of the paper are summarised and discussed.

2. Model and data used in this study

a. The modeling approach

We use the LODYC Ocean General Circulation Model (Madec et al. 1999) in a tropical Pacific configuration. The model is based on primitive equations (including potential temperature, horizontal currents, and salinity) solved by a finite difference scheme. Lateral mixing is applied along horizontal surfaces using a Laplacian operator with a 2000 $m^2\ s^{-1}$ coefficient. Vertical mixing is solved using the prognostic equation of turbulent kinetic energy (Blanke and Delecluse 1993). Solar radiation penetrates into the ocean according to an exponential profile. The model domain covers the tropical Pacific from 30°N to 30°S, 120°E to 75°W with realistic coastline and bathymetry. The zonal resolution is 1°. The meridional resolution varies from 0.5° in the equatorial waveguide to 2° at the northern and southern boundaries. There are 25 levels, with 10-m resolution down to 120 m. A time step of 5400 s is used.

A weekly wind stress product based on a combination of *European Remote-Sensing Satellite* (*ERS*) *1–2* scatterometer and Tropical Atmosphere–Ocean Array (TAO) data is used (Menkes et al. 1998). The heat and freshwater forcing is based on a monthly climatology derived from the European Centre for Medium-Range Weather Forecasts ERA-15 reanalysis (Gibson et al. 1997), with a seasonal flux correction. The interannual variations of the heat flux are approximated by including a $-15\ W\ m^{-2}\ K^{-1}$ relaxation to monthly SST climatology. No relaxation to sea surface salinity climatology is applied. This setup of the model is described in more detail Vialard et al. (2001, 2002), and has been shown to perform well during the 1993–99 period when compared to observations. The experiment above will be named REF (see Table 1).

b. Validation data

The Tropical Rainfall Measurement Mission (TRMM) Microwave Imager provides high-resolution and wide coverage SST measurements, whose space and time resolution allow one to analyze TIW properties (Chelton et al. 2000). We have retrieved TRMM SST weekly data for the May 1998–April 1999 period (see online at http://www.remss.com/) and have weight-averaged it to the model grid.

Subsurface temperature data from the TAO moorings will also be used to validate the model outputs. The depth of the 20°C isotherm deduced from TAO vertical temperature profiles will be compared against its model counterpart. The data and their description can be found online at http://www.pmel.noaa.gov/tao/.

c. Sensitivity experiments

In addition to experiment REF described earlier, we performed some sensitivity experiments. The ocean model is run a first time. It is then rerun with slightly different initial conditions. This allows one to test if the model TIW solution is strongly sensitive to initial conditions, that is, whether it is in a chaotic regime or not. The model initial conditions are its three-dimensional horizontal current, temperature and salinity fields. The perturbations to the initial conditions are constructed from a linear combination of model initial states.

In addition to the experiment REF described earlier using the full wind stress, some experiments using climatological wind stress will be described (see Table 1). One of these, denoted as SCY, uses an average seasonal cycle for the wind stress, constructed from the 1993–96 period, and smoothed with a 50-day low-pass filter. The heat and freshwater fluxes are as in experiment REF. The last experiment, denoted CST, uses a constant wind stress derived from the 1993–96 ERS–TAO wind stress average, and constant freshwater flux. The heat flux consists of a constant (climatological) part including a flux correction, augmented with a weak relaxation to a climatological annual mean temperature. To assess the robustness of the results obtained from the perturbation experiments to the reference experiment, we also ran perturbation experiments from CST and SCY.

d. Tropical instability wave analysis techniques

The main purpose of this paper is to study TIWs, which are manifest in several oceanic fields with period 20–40 days. A tenth-order digital filter using a Kaiser window was used to bandpass filter the daily outputs of the model in the range 10–50 days. Obviously, TIWs are not the only processes in this period band but they are the main contributor. This is particularly true for the SST field in the eastern Pacific, which exhibits clearly the TIW patterns.

A time-varying index of TIW activity can be defined based on the spatial root-mean-square (rms) value of the bandpass filtered SST over the TIW active region (0°–4°N, 100°–160°W, shown in Figs. 2 and 3). It is high when this box is occupied by large amplitude oscillation patterns. The thick line in Fig. 2a shows this index, corresponding to the SST field from the model experiment shown in Fig. 1a. It can be seen that the thick line captures well the TIWs level of activity, for example, the quiescent phases of the seasonal cycle or the low activity in 1997.

To examine the sensitivity of TIWs to initial conditions, we will use the following simple but robust way of quantifying the TIW phase and amplitude disagreement between two experiments (shown in Fig. 2a for the two experiments of Fig. 1). The spatial rms of the difference between the two 10–50-day filtered SST fields over the box defined above is representative of the TIW phase and amplitude agreement between the two experiments. When this value (thin curve) is well below the level of TIW activity (thick curve), TIWs are located at the same positions in the two experiments. If the thin curve reaches the thick one or goes above, then this means that significant phase and/or amplitude differences exist between the two experiments (the thin curve can reach twice the value of the thick one in the limit of signals of same amplitude but opposite phase). A strong disagreement between the TIWs of the control and perturbed experiments is suggested in 1993 and 1994, as confirmed by Fig. 1b. The method also captures the good agreement between TIWs in the perturbed and unperturbed experiments 1995 onward, and the temporary decline in this agreement at the end of 1996 due to differences close to 140°W as seen on Fig. 1b.

The diagnostic above measures both amplitude and phase agreement. Figure 2b shows the spatial correlation of the band-pass filtered SST of the perturbed and unperturbed experiments, computed over the same region. During 1995 and the end of 1996, this correlation is above 0.8, indicating an excellent TIW phase agreement of the two experiments (as can be seen in Figs. 1d and 1f for September 1995). At the same time, the thin line in Fig. 2a is at about half the value of the thick line, which might have been suggestive of a stronger phase disagreement. We will use the diagnostic shown in Fig. 2a to assess the phase and amplitude agreement between TIWs in two experiments, but will keep in mind that it is a stringent measure of this agreement.

3. The modeled and observed tropical instability waves

In this section, we compare the properties of TIWs in experiment REF with observations. Figure 3 highlights the main region of TIW activity in the SST observations and in the model, located around 2°N, in the vicinity of the mean position of the SST front. Both the model and observations depict TIW activity north of the equator from 85°W to 160°W and a weaker activity south of the equator (Chelton et al. 2000). The model captures the observed pattern of SST activity, but with slightly underestimated amplitude.

TIWs propagate westward with a phase speed of approximately 0.5 m s^{-1} in both the model and observations (Fig. 4). They appear as oscillations of the northern and southern edge of the cold tongue both in the model and in observations (Fig. 5). Also shown in Fig. 5b is a snapshot of the contemporaneous high-pass filtered model currents. The SST ridges north of the equator are clearly associated with anticyclonic vortices centered around 4.5°N, as observed by Kennan and Flament (2000) and Menkes et al. (2002) and in altimeter measurements by Weidman et al. (1999), with the northward movement of the cold tongue caused by a northward flow.

The TIWs are associated with strong variability in

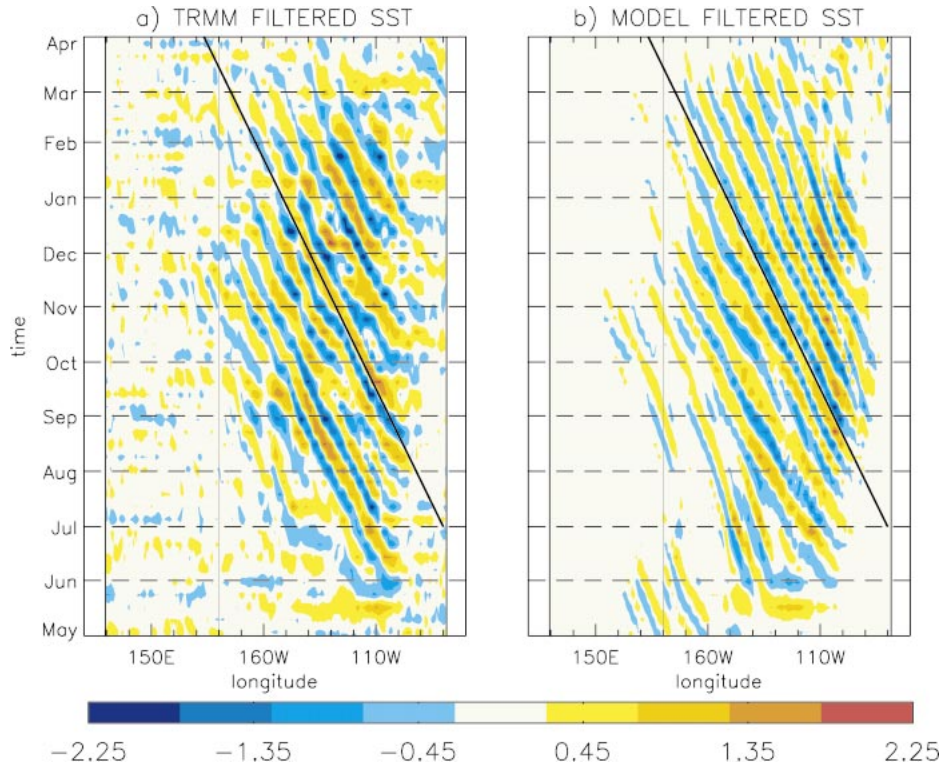

FIG. 4. Time–longitude section of 50-day high-pass filtered (a) observed TRMM SST and (b) modeled SST along 2°N for May 1998–Mar 1999. The thick line corresponds to a propagation speed of 0.5 m s^{-1}.

currents and dynamic height (Fig. 6). At 4.5°N (the central latitude of the vortices), there is a marked maximum in intraseasonal variability of the meridional speed and dynamic height (Figs. 6b and 6c), consistent with observed sea level (Perigaud 1990; McPhaden 1996). The maximum variability of the high-pass filtered zonal currents occurs at 2°N with a secondary peak around 6°N. This is consistent with vortices centered at 4.5°N, with stronger zonal currents on the southern side. The meridional speed has a secondary maximum in variability at the equator, most clearly seen around 120°W (Fig. 6b).

Figures 6d–f shows the vertical structure of the TIW activity along 140°W. The maximum of SST variability at 2°N associated with the meridional displacements of the mean SST front (Fig. 3) is also apparent in Fig. 6f. The temperature variability at 2°N is shallow. Around 5°N, the maximum of dynamic height variability seen in Fig. 6c is associated with subsurface temperature variability in the mean thermocline around 180 m. The zonal and meridional current maxima associated with the vortices have a significant contribution down to this depth. The equatorial maximum of meridional current variability is shallower, with no significant contribution below 100 m. The high frequency variability in the eastern and central Pacific thus consists of vortex-type variability down to 200 m north of the equator and shallower variability most prominent in the meridional current near the equator. The SST variability at 2°N is the result of the combined influence of these two types of current perturbations on the equatorial SST front.

In observations, the vortex-type variability north of the equator has a different timescale to the variability closer to the equator (Kennan and Flament 2000). In the model, at 140°W, the variability at the equator also has a higher frequency than the variability at 5°N (Fig. 7). The meridional current and dynamic height variability around 4.5°N are associated with a marked peak in the band 30–35 days, broadly in agreement with the peak found at 35–40 days in sea level observations. The variability in meridional currents closer to the equator is at a higher frequency than the vortices north of the equator. Even though the peak is not as clearly defined in the model (15–25 days), it is consistent with the one found near 20 days by Halpern et al. (1988) and Halpern (1989) in moored observations of meridional currents at the equator.

Figure 7 further shows that the model displays active and quiescent phases of the TIW activity. Active phases in the model are mostly prominent from July to January–March, depending on the year, in fair agreement with observations (Baturin and Niiler 1997). There is a strong interannual variability of the TIW activity level. The El Niño years display low

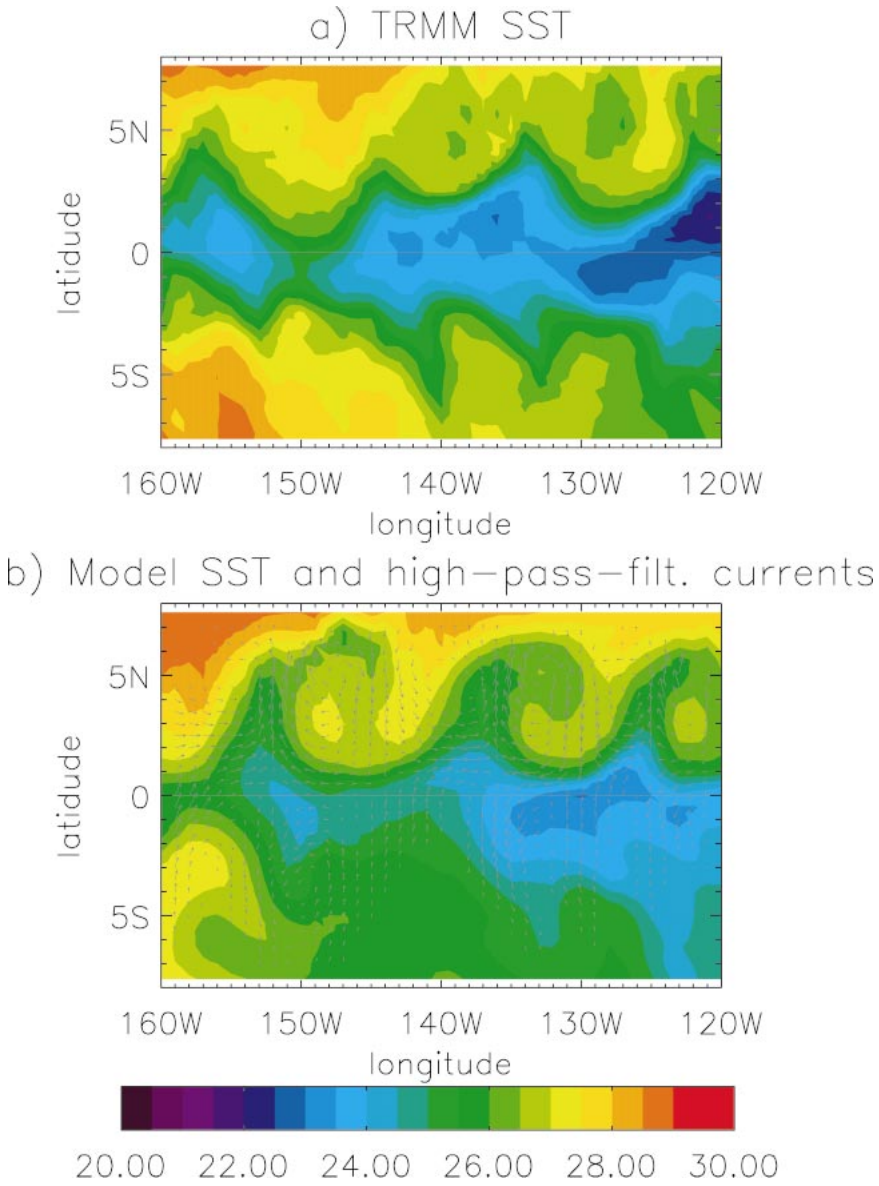

FIG. 5. Snapshot of (a) TRMM SST and (b) model SST for the first week of Nov 1998. The 50-day high-pass filtered model currents for the same week are drawn on (b).

TIW activity (Baturin and Niiler 1997), in particular during the 1997/98 winter. During the 1999 La Niña there is increased TIW activity in the model and in observations (Chavez et al. 1999).

To compare the levels of activity in the model and observations, we use TAO subsurface temperature in one of the strongest regions of TIW subsurface activity (5°N, 140°W). Figure 8 shows the model and observed vertical displacements 20°C isotherm at this location. There is general agreement between the model and observations, not only in terms of the low frequency variability, but also in terms of the level of activity of the TIWs and its seasonal and interannual variability.

We have thus shown that the model captures reasonably well the main observed TIW properties such as regions and patterns of variability, level of activity, and its temporal variation, timescale, and propagation speed.

4. Sensitivity of TIW phase to small perturbations in oceanic initial conditions

In this section, we investigate the dynamical regime of TIWs in the model by evaluating how sensitive they are to perturbations in the oceanic initial conditions.

In the first experiment, a small perturbation is added to the REF experiment on the first of January 1993. This

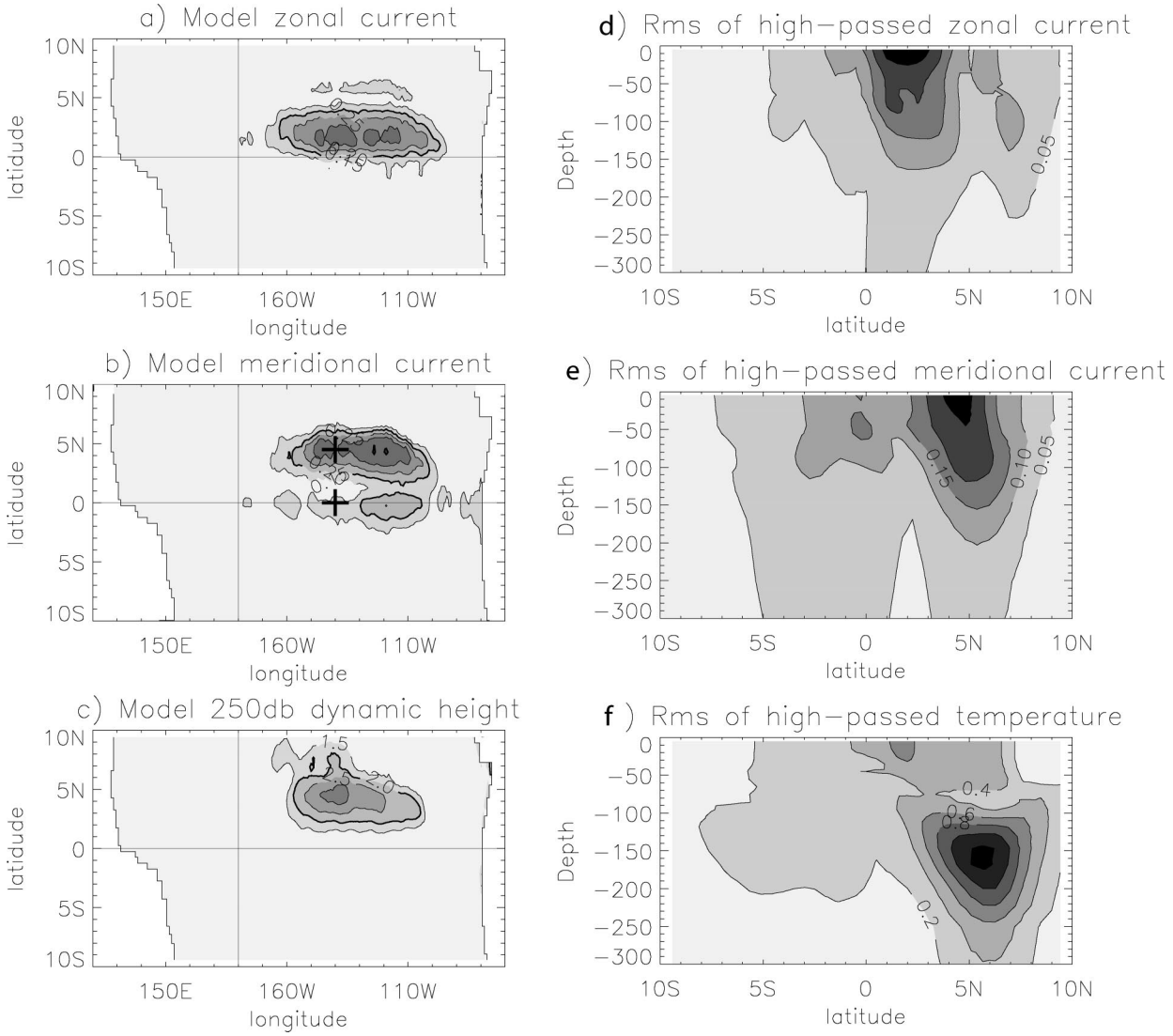

FIG. 6. Rms of 50-day high-pass filtered model variability of (a) surface zonal current, (b) surface meridional current, and (c) 250-dbar dynamic height. The two thick crosses on (b) indicate the positions corresponding to the time series and spectra of Fig. 7. Meridional sections at 140°W of the rms of 50-day high-pass filtered model fields are also shown for (a) zonal current, (b) meridional current, and (c) potential temperature.

perturbation is equal to 1/100 of the difference in oceanic initial state between 1 January 1993 and 1 June 1993. An ensemble of eight perturbation experiments using other initial perturbations was also run, but gave qualitatively similar results. The perturbed experiment is run over the whole 1993–mid-1999 period (i.e., many TIW cycles). Figure 9 is a measure of the phase agreement between TIWs in the unperturbed and perturbed experiments (see section 2d). Recall that TIWs are in good phase and amplitude agreement when the thin curve is well below the thick curve.

Over the first three years (i.e., after many TIW cycles) the TIW phase is in agreement in the REF and perturbed experiments (Fig. 9a). However, during active phases of the TIW season the trajectories of the perturbed and unperturbed experiments have a tendency to diverge slowly, and at the end of the fourth year there is a clear sign of phase disagreement between the REF and perturbed experiments at 140°W. At 110°W, however, the TIW activity remains correlated in the REF and perturbed experiments. The phase agreement over the whole box diminishes but not to the point where all correlation is lost (the correlation between the high-pass filtered SST of the two experiments over the whole box does not decrease below 0.7). This shows that the TIWs display some chaotic behavior, albeit a weak one. One might wonder why the phase agreement between the REF and perturbed experiments decreases more at the end of 1996 than during other years. This will be addressed in the discussion section of the paper.

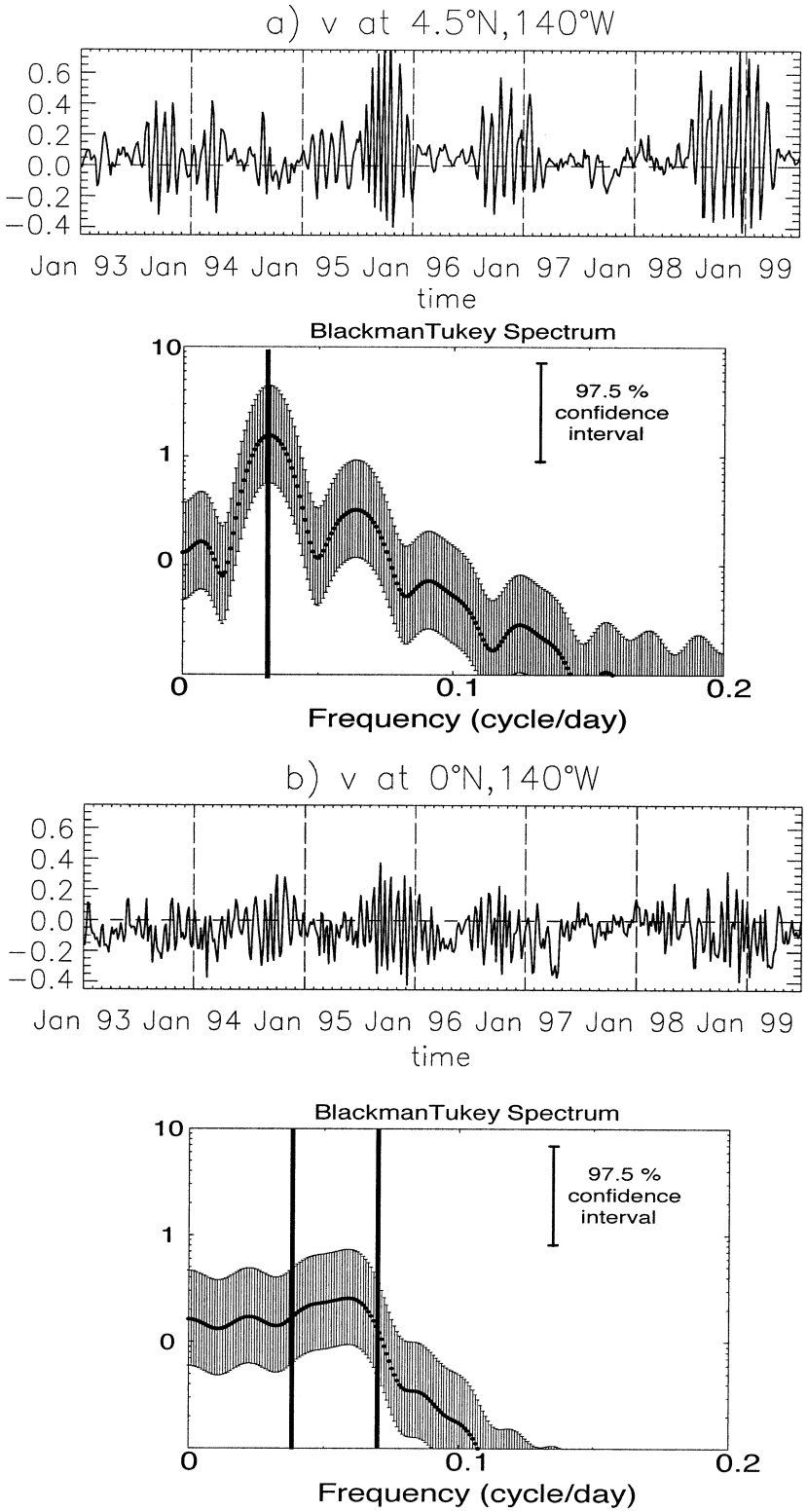

FIG. 7. Meridional currents of REF at 140°W: (a) the currents at 4.5°N and the corresponding spectrum (the vertical line indicates a 32-day period); (b) the time series and spectrum at the equator (the vertical lines indicate 15- and 25-day periods).

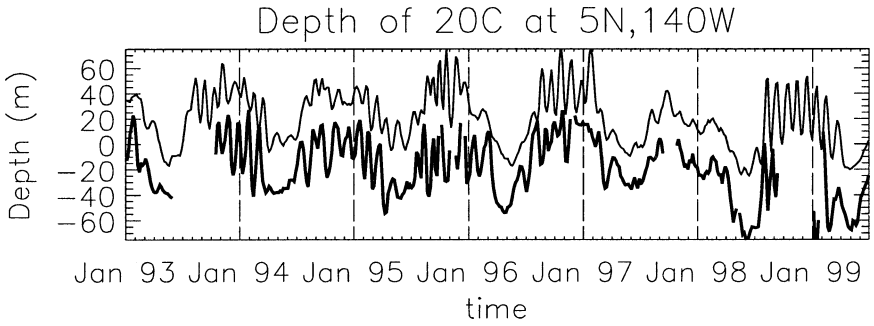

FIG. 8. Depth of the 20°C isotherm at 5°N, 140°W in the model (thin line) and TAO data (thick line). The mean value of each series has been removed. The curves have been offset by ±20 m, respectively, for display purposes.

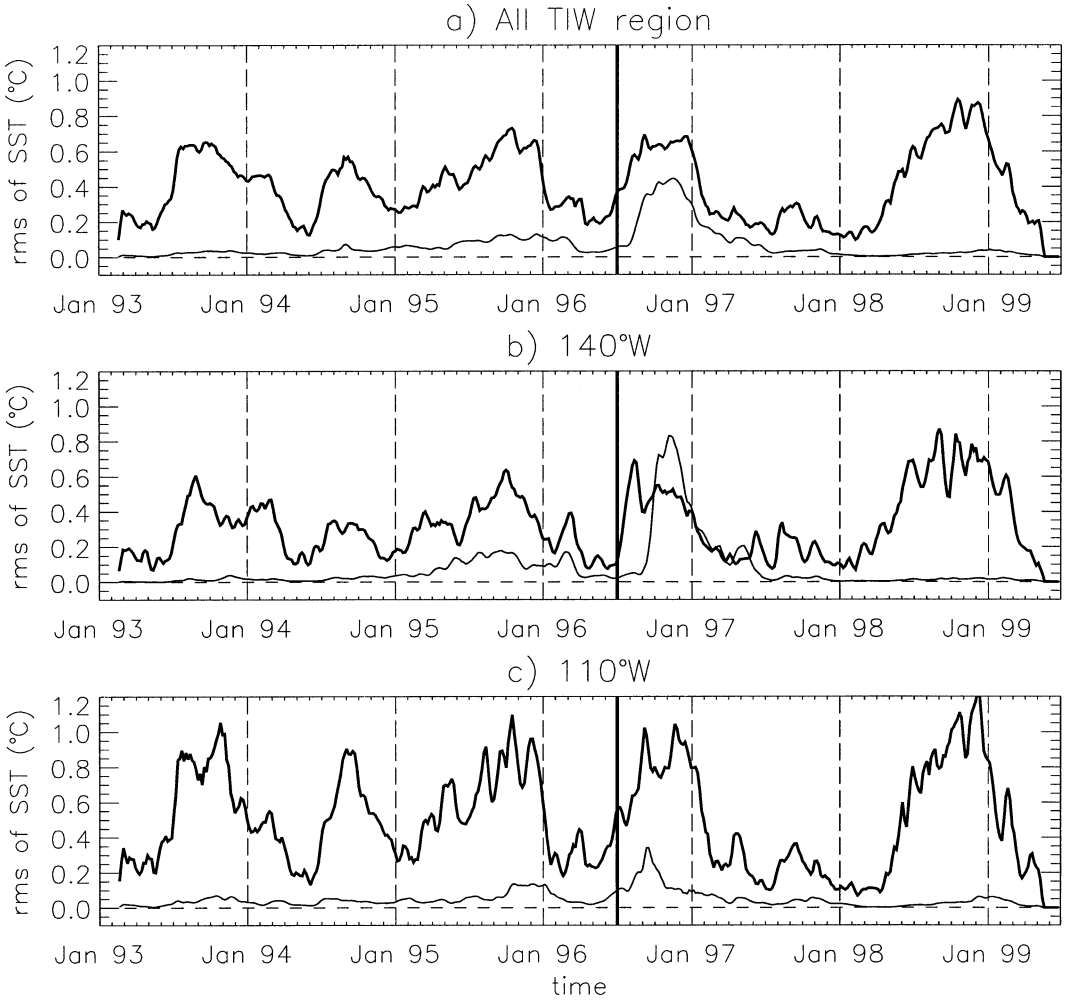

FIG. 9. Level of activity of TIWs in REF (thick line) and phase agreement between TIWs in the REF and in an experiment with a small perturbation to the initial conditions applied in Jan 1993 (thin line) (a) for the whole TIW region, as in Fig. 2, and (b), (c) for two 10°-lon-wide, 0°–4°N boxes centered at 140° and 110°W, respectively. The level of activity and phase agreement are estimated as in Fig. 2a, and as described in section 2d.

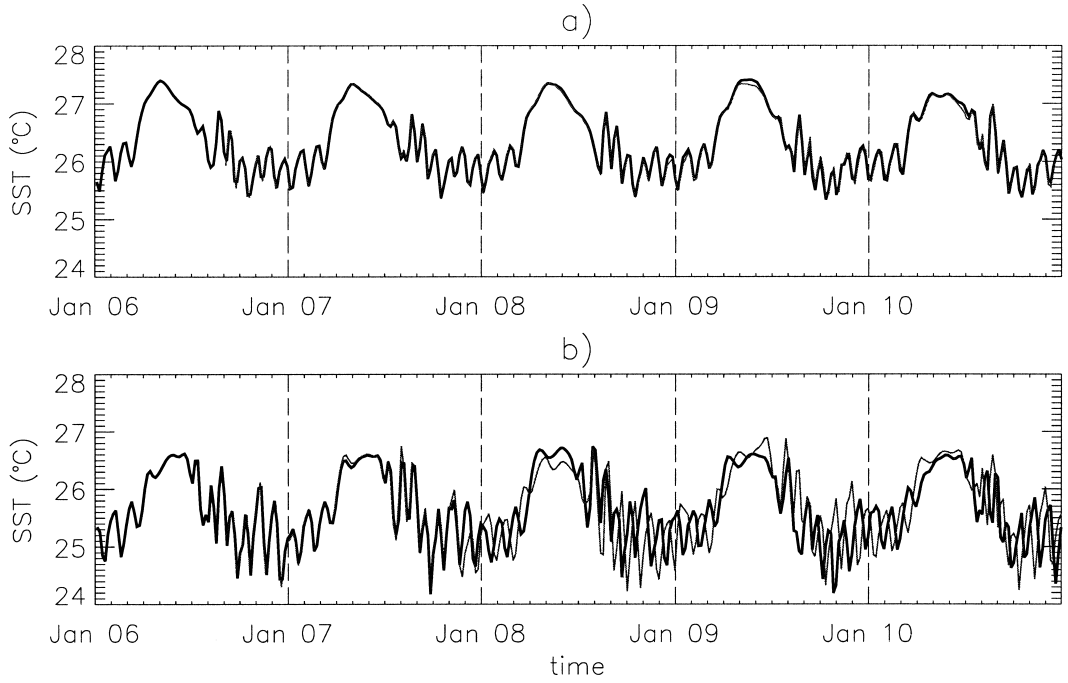

FIG. 10. (a) Temperature at 2°N, 140°W of the SCY expt (using a climatological seasonal cycle of the wind) shown as a thick line. The thin line is a perturbation experiment, with a *small* perturbation applied at the beginning of Sep year 6 (first year on the plot). This line is barely visible since it almost overlies the thick line. (b) Similar control and perturbation experiments are shown, but using the SCY wind stress multiplied by 1.5.

Figure 9 also illustrates that the TIW phase agreement between the two experiments is linked with the level of TIW activity. When TIWs are active, the difference between the two experiments grows (e.g., end of 1993, from June 1994 to the end of 1995, and at the end of 1998). Conversely, during quiescent phases of the TIW activity, the two experiments tend to come back into phase: for example, during the low TIW activity period associated with the 1997–98 El Niño. This can be understood in the following way. When easterlies weaken as a result of the seasonal cycle or an El Niño, all factors contributing to the instability mechanisms (current shear, temperature gradient between the cold tongue and water to the north) are diminished, the equatorial current system is less prone to instabilities, and perturbations decay.

Additional experiments applying various perturbations at the beginning of the TIW season (with rms amplitude of around 0.05°C over the TIW region) were run for each year from 1993 to 1998. For most years, these perturbations do not grow enough to change radically the TIW phase over the season. These experiments thus reinforced the conclusion that TIW activity is only weakly chaotic in experiment REF.

To provide an illustration of the results presented above in a simpler framework and to assess their robustness, we added some perturbations to experiment SCY using an average seasonal cycle of the winds. At the begining of the sixth year of this experiment, a small perturbation, equal to 1/100 of the difference between the 1 January and 1 July of year 6, was added. (Other experiments with different small perturbations gave similar results.) Figure 10a compares the SST of the perturbed and unperturbed experiments at one point in the central Pacific. Even after several years, the two curves lie almost exactly on top of each other. The phase agreement between the control and perturbed experiment remains in good agreement not only at this location but over the whole region where TIWs appear and up to year 10. This illustrates that TIW activity in experiment SCY is close to a stable limit cycle behavior. Some small differences can however be spotted between the perturbed and unperturbed trajectories after a few years, maybe illustrative of weakly chaotic behavior (but the Lyapunov exponent characteristic of the chaos is certainly small because the phase agreement is still almost perfect after four years and many TIWs cycles). As a matter of fact, the result of the perturbation experiment could be deduced from the SCY experiment itself. In this experiment, the TIWs repeat almost exactly in the same way and with the same phase from one year to the next. This regularity is suggestive of the absence of chaos, and thus of little sensitivity to initial conditions. This intriguing behavior will be discussed in more detail in section 6b.

These results indicate that TIWs do not exhibit a strong chaotic behavior in our experiments, but one closer to a limit cycle. However, McCreary and Yu (1992) found that the TIW regime could be sensitive to model parameters, such as horizontal mixing or the strength

of wind stress. To investigate this sensitivity, we repeated the SCY experiment with increased wind stress (multiplied by 1.5). By doing this, the surface circulation and its horizontal shear as well as the thermocline tilt; that is, the generating factors of TIWs are increased. This results in stronger TIW variability (Fig. 10b). The TIW activity not only becomes stronger but also less regular: TIWs no longer repeat in the same way from one year to the next. Consistent with this, a perturbation experiment (similar to the one of Fig. 10a) shows a greater sensitivity to initial conditions. The phase between the control and the perturbation experiments is completely lost after about 14 months and is never recovered (Fig. 10b). This is characteristic of chaotic behavior. It is surprising, however, that in this experiment, it takes about 14 months for the perturbation to grow from its initial size of $O(10^{-2})$°C to about 1°C. The *e*-folding time of perturbation growth (about 120 days) seems much longer than the *e*-folding growth rate of TIWs themselves (of the order of 10–20 days: e.g., (McCreary and Yu 1992). This could be linked to the fact that the linear instability of the flow is weaker when linearizing about a state including TIWs than when linearizing about the mean state. This experiment illustrates that the TIW behavior in the model can be made more chaotic by increasing the wind strength. It should be pointed out, however, that the wind stress product becomes unrealistically strong when multiplied by 1.5. We will come back to this point in the discussion.

We have discussed the dynamical regime of TIWs for an experiment with observed winds and with a seasonal cycle. We will now turn to an even simpler case with constant winds (see Table 1 and section 2c). Figure 11a shows the evolution of SST in the CST experiment at 140°W. As in the SCY experiment, it illustrates a highly regular behavior, although there is some sign of amplitude modulation. The absence of a chaotic behavior is confirmed by the perturbation experiment. As in the REF and SCY experiments, hardly any sign of perturbation growth is spotted, even after many TIW cycles.

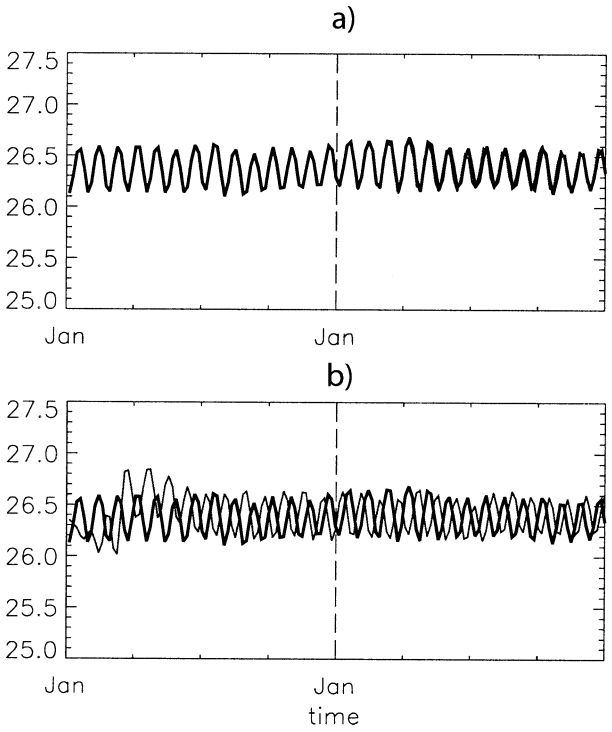

FIG. 11. Temperature at 2°N, 140°W of the CST experiment (using a climatological annual mean of the wind) shown as a thick line. (a) The thin line is a perturbation experiment with a *small* perturbation applied at the beginning of Sep year 6 (first year on the plot). This line is barely visible since it almost overlies the thick line. (b) The thin line is a perturbation experiment with a *large* perturbation applied at the beginning of Sep year 6.

5. Sensitivity of TIW phase to large perturbations to oceanic initial conditions

In the previous section, we investigated the stability of TIWs to small perturbations and showed that the TIWs generally exhibited little sensitivity to initial conditions. In this section, we will examine what happens if we apply large perturbations to the initial conditions. We have seen in the REF, SCY, and CST experiments with realistic wind strength, that the system behavior was weakly chaotic, close to a stable limit cycle. Let us now discuss briefly the expected behavior of such a system to small and large perturbations. If a small perturbation is applied to a system in a perfect stable limit cycle, the system will return to this limit cycle. The perturbation being small, it will only take the system a short time to return to the limit cycle and the phase shift introduced by the perturbation will be, and will remain, small. This description is consistent with the one that was observed in Fig. 11a. If a large perturbation is introduced, it will take longer for the perturbed system to return to its limit cycle, potentially introducing a larger phase shift between the perturbed and unperturbed trajectories. Figure 11b shows the SST of the CST experiment again. Another experiment is started from the long term average of the CST experiment and thus close to the ''center'' of the limit cycle. The typical amplitude of the perturbation is large: about 1°C. Once again, the expected behavior is observed: after an initial adjustment during a few TIW periods, the perturbed trajectory adjusts back to oscillations of similar amplitude and period to the CST experiment, but with a phase shift. This phase shift then remains approximately constant in time.

A different behavior is observed when the previous experiment is repeated using a seasonal cycle of the winds. The SCY experiment was restarted from its long-term average (average of years 6–10) on 1 September of the sixth year (Fig. 12). This corresponds to a large perturbation (with a magnitude of several degrees in temperature). The perturbed experiment first experiences an adjustment phase, the timescale of which is fixed

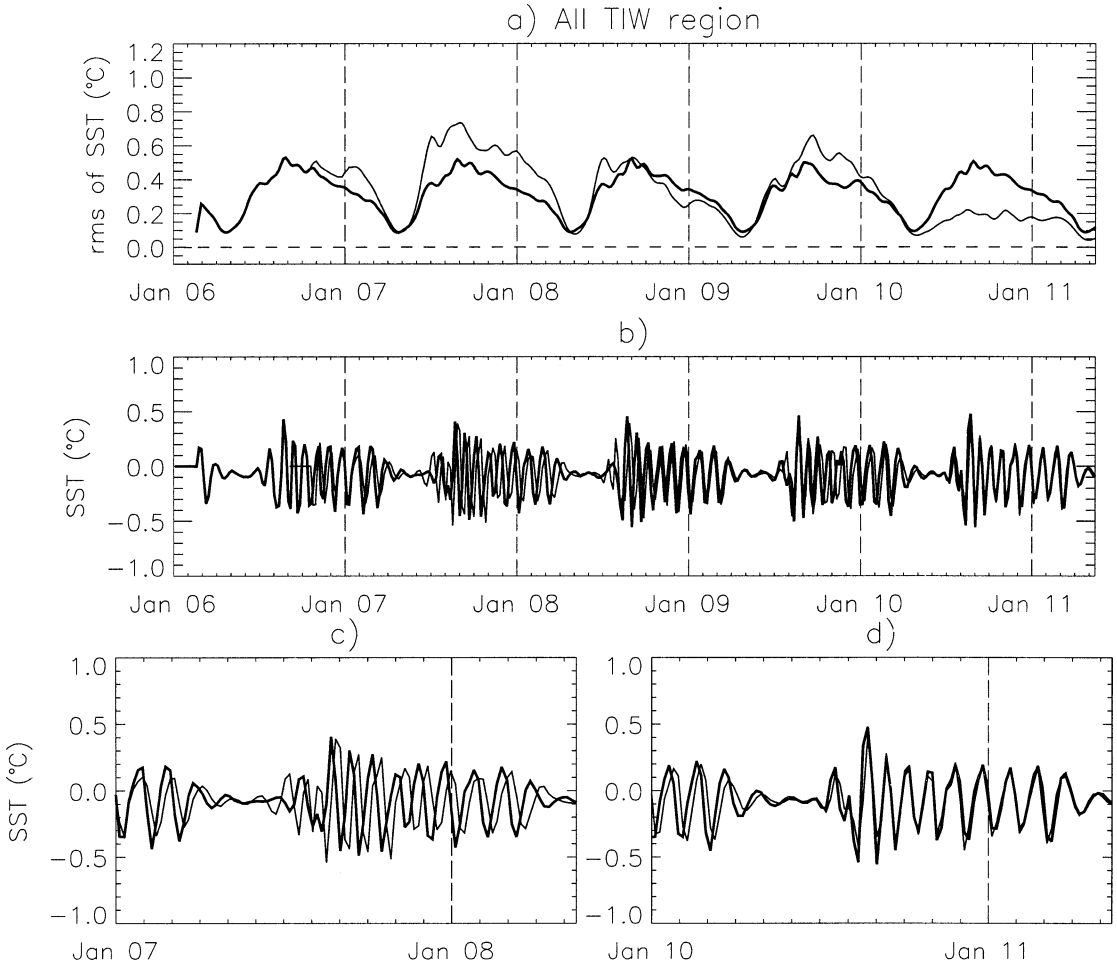

FIG. 12. (a) As for Fig. 9a but for expt SCY and a perturbation experiment with a *large* perturbation applied at the beginning of Sep year 6 (first year on the plot). (b) The time series of the SST of the SCY and perturbed experiments at 2°N, 140°W for the whole period; and (c), (d) blow-ups of shorter periods.

by the time it takes equatorial waves to carry information across the basin. This initially results in a completely different phase of the TIWs in the perturbed and control experiments (Fig. 12c). From the previous experiment with constant winds, one could expect this phase shift in the TIWs to remain. But surprisingly, the TIWs in the control and perturbed experiments have a tendency to come back into phase after several years. Figure 12a measures the phase agreement of the two experiments over the whole TIW region. Figures 12a and 12d illustrate that a good phase agreement is regained over the whole TIW-active region after four years. The good phase agreement between the two experiments is maintained beyond year 10. In contrast with the experiment shown in Fig. 11b, Fig. 12 shows that the introduction of the seasonal cycle can bring the perturbed and unperturbed trajectories into phase. This is consistent with Allen et al. (1995) and Benestad et al. (2001), who proposed that the TIW phase could be locked to wind variations. More precisely, these authors suggested that the TIW phase could be locked to intraseasonal variations of the wind forcing. Our results here suggest that the TIW phase can also be locked to the seasonal cycle of the wind. We will discuss in more detail the potential mechanisms of this phase locking at the end of the paper.

Last, we tested if the phase locking of the TIWs to the wind would persist in the presence of the full wind forcing. The REF experiment was thus restarted from its long-term average on 1 September 1993 (other large perturbations were applied at other dates and gave consistent results). This is the perturbation experiment that was shown in Fig. 1. As already discussed, after an initial phase disagreement between the TIWs in the two experiments, they later come back into phase (the phase agreement is rather good from 1995—the third year—onward). In 1998 and 1999, this phase agreement is excellent, both at 140°W and over the whole domain. In 1996, there is phase disagreement around 140°W because one TIW in the REF experiment splits into two in the perturbed experiment (in October–November 1996, Fig. 13d), but this disagreement stays localized

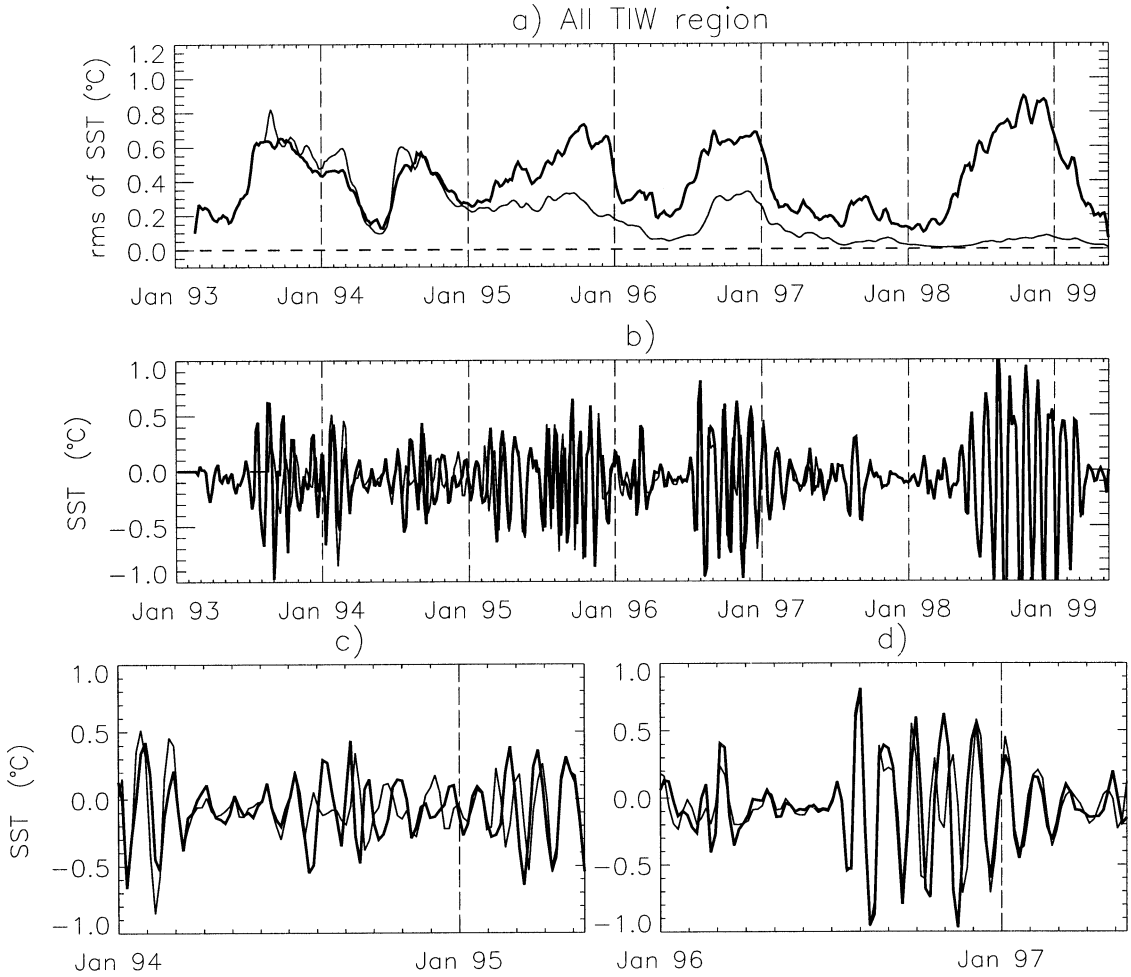

FIG. 13. As for Fig. 12 but for expt REF and a perturbation experiment with a *large* perturbation applied at the beginning of Sep 1993 (first year on the plot).

in time and space. This suggests that some chaotic behavior (albeit weak) is still at work and might be associated with situations favorable to TIW splitting. However, the overall behavior of the system is dominated by a phase locking of TIWs to the background flow. This phase locking is much clearer in the case with the full wind forcing than in the case with the climatological seasonal cycle, as illustrated by comparison of Figs. 12a and 13a. This suggests that components other than the seasonal cycle are important for locking the phase of the TIWs. Complementary experiments filtering out various components (intraseasonal, seasonal, and interannual) of the wind forcing show that all these components contribute to the phase locking, which is strongest with the full winds.

6. Summary and discussion

a. Summary

In this study, we have shown that the LODYC OGCM can reproduce the main features of TIWs variability in the central and eastern Pacific. TIWs are manifest on snapshots of the SST field as undulations of the equatorial SST front and propagate westward at 0.5 m s^{-1} both in the model and observations. The model displays variability with period 30–35 day north of the equator (against 35–40 day in observations). The current shows a vortexlike structure centered at about 4.5°N. The current variability is maximum close to the surface and extends down to the mean thermocline (between 150 and 200 m) where temperature variability is greatest. Validation of the model thermocline depth in a region of active TIWs (at 5°N, 140°W) shows good agreement with TAO data in terms of level of activity.

In addition to the vortex-type variability north of the equator, there is activity at a shorter period near the equator, in both the model (15–25 day) and observations (around 20 days: Halpern et al. 1988; Halpern 1989) but more sharply defined in observations. The intraseasonal current at the equator is not coherent with the vortex-type variability at 4.5°N, neither in observations (e.g., Kennan and Flament 2000) nor in our experiments

(e.g., Fig. 7). The equatorial activity is most prominent in the near-surface meridional currents. The SST variability at 2°N is the result of the combined effects of the equatorial- and vortex-type activity on the equatorial front. Finally, the model reproduces well the active and quiescent phases of TIW variability linked with the seasonal cycle and interannual variability.

Since the model is successful at reproducing many aspects of the observed TIW field, we used it to investigate the dynamical regime of TIWs by investigating their sensitivity to perturbations in initial conditions. It is found that TIWs exhibit little sensitivity to small perturbations in oceanic initial conditions. Small differences sometimes grow locally in space and time (i.e., a few TIW cusps can be located differently in the control and perturbed experiments), but never enough to significantly harm the phase agreement over the whole active TIW region. The differences only develop after a time long compared to the timescale of TIWs themselves, and never grow enough to result in a complete inconsistency of the phases of the control and perturbed experiments.

The phase of the TIWs is repeated nearly exactly in the same way from one year to the next in experiments using a seasonal cycle forcing, which suggests phase locking of TIWs to the forcing. This is confirmed by experiments, using much larger perturbations to the oceanic initial conditions. In these experiments, the perturbations are large enough to result in TIWs that are completely uncorrelated between the control and perturbed experiments during the early adjustment period. As the integration proceeds, this phase difference decreases with time and disappears. This phase locking is clearest when using the full spectrum of the winds. In the case of constant wind forcing, there is obviously no phase locking.

b. Discussion

Before discussing in more detail the results obtained in this paper, we will point out a few caveats of this study. First, these results show that TIW variability is phase locked to the wind forcing. With a perfect model and forcing, one would thus expect the phase of TIWs in the model to be consistent with observed TIWs. This is not the case, however, in our experiments because the spatial and temporal scales of the TIWs are slightly different in the model and observations, probably due to the thermocline being too diffuse and the undercurrent and North Equatorial Counter Current slightly too weak (Vialard et al. 2001). Some aspects of the TIWs physics might also be neglected here. For example, Chelton et al. (2001) and Hashizume et al. (2001) showed that coupling with the planetary boundary layer generates a TIW signature in the surface wind stress. This signature is not clearly reproduced in the wind stress products we were using.

This study revealed that TIW phase is only weakly sensitive to perturbations to initial conditions. This is consistent with a limit cycle behavior. In the simulations using realistic wind forcing, the irregularities in phase and amplitude of TIWs are thus linked to external forcing rather than to internal dynamics. A stronger result is that the phase of TIWs is locked to the wind forcing. It was shown in section 4 and in McCreary and Yu (1992) that modeled TIWs could be made more chaotic, for instance, by increasing the wind forcing. One might wonder if the model is representative of the TIWs regime in the real world. First, section 3 shows that TIW properties in the model are in reasonable agreement with those observed. Further, the results about the phase locking are robust. They are preserved when using different wind products (FSU stresses, with a rather strong drag coefficient of 1.5×10^{-3}), or ERS–TAO stresses multiplied by 1.2. The latter wind forcing has to be made unrealistically strong (multiplied by 1.5) to result in a chaotic behavior. We thus think that the results obtained in this paper might be relevant to describe the dynamical properties of observed TIWs.

These results are not inconsistent with the fact that TIWs are generated by instability processes. These results only suggest that the system is stable when linearised around a trajectory including TIWs. This does not contradict the fact that TIWs themselves are the result of an instability.

The mechanism of the phase locking needs to be understood. The quiescent phases of the seasonal cycle (and occasional inactive periods linked to an El Niño) play an essential role in the absence of long-term sensitivity of the TIW phase to initial conditions. Indeed, during these periods, the state of the system does not sustain instability growth and perturbations to the TIW field are damped. In the experiment with increased wind, the year to year growth of the TIW field perturbation might be associated to the fact that the minimum wind stress, during the quiescent boereal spring period, is now above the critical level for chaos. The quiescent phase of the seasonal cycle is thus important to explain the absence of strong sensitivity to initial conditions, but cannot explain TIW phase locking. Around June each year, the mean flow becomes unstable. Background noise can thus be amplified in the region of unstable flow, which then leads to the development of TIWs. If the unstable region has a large zonal extent, one expects the phase of TIWs to be random since they depend on the initial distribution of background noise in this region. Since the phases are not random, there must be an additional mechanism that forces the first TIW of the season to always appear at a precise location with a precise timing. A possible reason to explain this is that localized growth of the instability in space and time can appear when the background flow characteristics reach some critical threshold. This localized growth of the instabilities would force the TIWs to appear at precise locations.

To better understand the phase locking mechanism,

one needs to understand how the large-scale parameters of the background flow (current shear, pressure gradients) control the short-term growth rate of the instabilities. Generalized stability theory (Farrel and Ioannou 1996) provides a general framework to describe the short-term growth of instabilities and investigate the control of the growth rate by the background flow. We will thus pursue this study using generalized stability theory. In particular, this could allow to understand why the various experiments can sometimes display localized perturbation growth (e.g., at 140°W at the end of 1996 in experiment REF).

This study suggests that TIWs are only weakly sensitive to initial conditions and strongly phase locked to the variability of the background flow produced by the external atmospheric forcing. This might have a few practical consequences. For example, it suggests that, if TIWs are produced with the correct time and spatial scale, ocean models forced by observed forcing should be able to reproduce them with the correct phase, as suggested by Allen et al. (1995). In particular, this will apply to data assimilation studies, which should be able to reconstruct the observed phase of the TIWs using the combined informations from the wind forcing and ocean data. Indeed, Seidel and Giese (1999) and Weaver et al. (2002) have shown that TIWs can be generated with a correct phase with the help of data assimilation.

Acknowledgments. We thank J. P. McCreary, W. Kessler, T. Stockdale, K. Richards, and R. Sutton for useful discussions. D. Chelton and an anonymous reviewer provided *very* useful comments that allowed us to improve the manuscript substantially. J. Vialard and C. Menkes are funded by IRD (Institut de Recherche pour le Developpement). The spectra in Fig. 7 were computed using the SSA-MTM Toolkit developed in the Department of Atmospheric Sciences of the University of California, Los Angeles. The plotting package used in all other plots is based on IDL™ and has been developed by S. Masson.

REFERENCES

Allen, M. R., S. P. Lawrence, M. J. Murray, C. T. Mutlow, T. N. Stockdale, D. T. Llewellyn-Jones, and D. L. T. Anderson, 1995: Control of tropical instability waves in the Pacific. *Geophys. Res. Lett.,* **22,** 2581–2584.

Baturin, N. G., and P. P. Niiler, 1997: Effect of instability waves in the mixed layer of the equatorial Pacific. *J. Geophys. Res.,* **102,** 27 771–27 793.

Benestad, R. E., R. T. Sutton, M. R. Allen, and D. L. T. Anderson, 2001: The influence of subseasonal wind variability on tropical instability waves in the Pacific. *Geophys. Res. Lett.,* **28,** 2041–2044.

Blanke, B., and P. Delecluse, 1993: Variability of the tropical Atlantic ocean simulated by a general circulation model with two different mixed layer physics. *J. Phys. Oceanogr.,* **23,** 1363–1388.

Chavez, F. P., P. G. Strutton, G. E. Friedrich, R. A. Feely, G. C. Feldman, D. G. Foley, and M. J. McPhaden, 1999: Biological and chemical response of the equatorial Pacific Ocean to the 1997–1998 El Niño. *Science,* **286,** 2126–2131.

Chelton, D. B., F. J. Wentz, C. L. Gentemann, R. A. de Skoeze, and M. G. Schlax, 2000: Satellite microwave SST observations of transequatorial tropical instability waves. *Geophys. Res. Lett.,* **27,** 1239–1242.

——, and Coauthors, 2001: Observations of coupling between surface wind stress and sea surface temperature in estern tropical Pacific. *J. Climate,* **14,** 1479–1498.

Cox, M. D., 1980: Generation and propagation of 30-day waves in a numerical model of the Pacific. *J. Phys. Oceanogr.,* **10,** 1168–1186.

Donohue, K. A., and M. Wimbush, 1998: Model results of flow instabilities in the tropical Pacific Ocean. *J. Geophys. Res.,* **103,** 21 401–21 412.

Farrel, B. F., and P. J. Ioannou, 1996: Generalized stability theory. Part II: Nonautonomous operators. *J. Atmos. Sci.,* **53,** 2041–2053.

Flament, P., A. C. Kennan, R. A. Knox, P. P. Niiler, and R. L. Bernstein, 1996: The three-dimensional structure of an upper ocean vortex in the tropical Pacific. *Nature,* **383,** 610–613.

Gibson, J. K., P. Kallberg, S. Uppala, A. Nomura, A. Hernandez, and E. Serrano, 1997: ERA description. ECMWF reanalysis final rep. series 1, 71 pp.

Halpern, D., 1989: Detection of 17.5-day period meridional current oscillations in the equatorial western Pacific Ocean during 1985. *Geophys. Res. Lett.,* **16,** 499–502.

——, R. A. Knox, and D. S. Luther, 1988: Observations of 20-day period meridional current oscillations in the upper ocean along the Pacific equator. *J. Phys. Oceanogr.,* **18,** 1514–1534.

Hashizume, H., S.-P. Xie, W. T. Liu, and K. Takeuchi, 2001: Local and remote atmospheric response to tropical instability waves: A global view from space. *J. Geophys. Res.,* **106,** 10 173–10 185.

Kennan, S. C., and P. J. Flament, 2000: Observations of a tropical instability vortex. *J. Phys. Oceanogr.,* **30,** 2277–2301.

Legeckis, R., 1977: Long waves in the equatorial Pacific Ocean. A view from a geostationary satellite. *Science,* **197,** 1179–1181.

Luther, D. S., and E. S. Johnson, 1990: Eddy energetics in the upper equatorial Pacific during the Hawaii-to-Tahiti Shuttle Experiment. *J. Phys. Oceanogr.,* **20,** 913–944.

Madec, G., P. Delecluse, M. Imbard, and C. Levy, 1999: OPA 8.1 ocean general circulation model reference manual. Notes du pôle de modélisation 11, Institut Pierre Simon Laplace (IPSL), 91 pp.

Masina, S., S. G. H. Philander, and A. B. G. Bush, 1999: An analysis of tropical instability waves in a numerical model of the Pacific Ocean. 2: Generation and energetics of the waves. *J. Geophys. Res.,* **104,** 29 637–29 661.

McCreary, J. P., Jr., and Z. Yu, 1992: Equatorial dynamics in a 2.5-layer model. *Progress in Oceanography,* Vol. 29, Pergamon, 61–132.

McPhaden, M. J., 1996: Monthly period oscillations in the Pacific North Equatorial Countercurrent. *J. Geophys. Res.,* **101,** 6337–6359.

Menkes, C., J. P. Boulanger, A. J. Busalacchi, J. Vialard, P. Delecluse, M. J. McPhaden, E. Hackert, and N. Grima, 1998: Impact of TAO vs ERS wind stress onto simulations of the tropical Pacific Ocean during the 1993–1998 period by the OPA OGCM. Euroclivar Workshop Rep. 13, 46–48.

——, and Coauthors, 2002: A whirling ecosystem in the equatorial Atlantic. *Geophys. Res. Lett.,* **29,** 1553, doi:10.1029/2001GL014576.

Murray, W. J., R. T. Barber, M. R. Roman, M. P. Bacon, and R. A. Feely, 1994: Physical and biological controls on carbon cycling in the equatorial Pacific. *Science,* **266,** 58–65.

Perigaud, C., 1990: Sea level oscillations observed with Geosat along the two shear fronts of the Pacific North Equatorial Countercurrent. *J. Geophys. Res.,* **95,** 7239–7248.

Qiao, L., and R. H. Weisberg, 1998: Tropical instability wave energetics: Observations from the Tropical Instability Wave Experiment. *J. Phys. Oceanogr.,* **28,** 345–360.

Seidel, H., and B. S. Giese, 1999: Equatorial currents in the Pacific Ocean, 1992–1997. *J. Geophys. Res.,* **104,** 7849–7863.

Strogatz, S. H., 1994: *Nonlinear Dynamics and Chaos with Applications in Physics, Biology, Chemistry, and Engineering.* Perseus Press, 498 pp.

Swenson, M. S., and D. V. Hansen, 1999: Tropical Pacific Ocean mixed layer heat budget: The Pacific cold tongue. *J. Phys. Oceanogr.*, **29,** 69–81.

Vialard, J., C. Menkes, J.-P. Boulanger, P. Delecluse, E. Guilyardi, M. J. McPhaden, and G. Madec, 2001: A model study of oceanic mechanisms affecting the equatorial Pacific sea surface temperature during the 1997–98 El Niño. *J. Phys. Oceanogr.*, **31,** 1649–1675.

——, P. Delecluse, and C. Menkes, 2002: A modeling study of salinity variability and its effects in the Pacific Ocean during the 1993-99 period. *J. Geophys. Res.*, **107** (C12), 8005, doi:10.1029/2000JC000758.

Weaver, A. T., J. Vialard, D. L. T. Anderson, and P. Delecluse, 2002: Three- and four-dimensional variational assimilation with a general circulation model of the tropical Pacific Ocean. ECMWF Tech. Memo., 365, 76 pp.

Weidman, P. D., D. L. Mickler, B. Dayyani, and G. H. Born, 1999: Analysis of Legeckis eddies in the near-equatorial Pacific. *J. Geophys. Res.*, **104,** 7865–7887.